Nuclear Spin Gyroscope based on the Nitrogen Vacancy Center in Diamond

Vladimir V. Soshenko[1,2] Stepan V. Bolshedvorskii,[1,2,3] Olga Rubinas,[1,2,3] Vadim N. Sorokin,[1]
Andrey N. Smolyaninov,[2] Vadim V. Vorobyov,[1,4] and Alexey V. Akimov[1,5,*]

[1]P. N. Lebedev Physical Institute, 53 Leninskij Prospekt, Moscow 119991, Russia
[2]LLC Sensor Spin Technologies, The Territory of Skolkovo Innovation Center, Street Nobel b.7, Moscow 143026, Russia
[3]Moscow Institute of Physics and Technology, 9 Institutskiy per., Dolgoprudny, Moscow Region 141700, Russia
[4]3rd Institut of Physics, IQST and Centre for Applied Quantum Technologies, University of Stuttgart,
Pfaffenwaldring 57, Stuttgart 70569, Germany
[5]Texas A&M University, 4242 TAMU, College Station, Texas 77843, USA

A rotation sensor is one of the key elements of inertial navigation systems and compliments most cell phone sensor sets used for various applications. Currently, inexpensive and efficient solutions are mechanoelectronic devices, which nevertheless lack long-term stability. Realization of rotation sensors based on spins of fundamental particles may become a drift-free alternative to such devices. Here, we carry out a proof-of-concept experiment, demonstrating rotation measurements on a rotating setup utilizing nuclear spins of an ensemble of nitrogen vacancy centers as a sensing element with no stationary reference. The measurement is verified by a commercially available microelectromechanical system gyroscope.

With the increasing interest in unmanned and autonomous vehicles, inertial navigation becomes of pivotal importance for steering in areas lacking global navigation system signals, for example, inside buildings or tunnels and under water or ground [1–3]. The records for precision and bias stability of industrially available gyroscopes are traditionally held by ring-laser gyroscopes and fiber-optic gyroscopes, the ideas of which were developed by the end of the 20th century [4–8]. Based on the Sagnac effect, their precision is proportional to the surface enclosed by the optical light path [9,10]. While there has been great progress in miniaturization of this type of device [11], fundamental limits, related to the size and sensitivity of the device, are still hard to overcome. On the other hand, much less precise microelectromechanical system (MEMS) gyroscopes are widely used for mass production in consumer electronics. While the bias stability of these devices is often not sufficient for robust long-term inertial navigation, these devices have excellent power consumption characteristics, chip-scale dimensions and low prices [12]. Despite enormous progress in improving the bias stability and precision of these devices, there is still a considerable gap between compact and precise devices. As an attempt to bridge the gap, redesigning laser-based gyroscopes by trying to use chip-scale high quality factor cavities [11,13] is currently at the stage of implementing prototypes capable of measuring the earth rotation rate. Another competing approach allowing combination of compact in size sensor and close to a state-of-the-art precision is the development of hyperpolarized noble gas nuclear spin gyroscopes [14–18]. Thus, it seem natural to consider solid-state spin systems as well.

The nitrogen vacancy (NV) center in diamond possesses optically detectable electron spin, with a long coherence time at room temperature and means for optical polarization of the spin state. The NV center was already used in nuclear magnetic resonance spectroscopy with chemical resolution [19,20] and as a sensor of magnetic [21–23] and electric [24] fields as well as temperature [25].

In 2012, it was proposed [26–28] to use an NV center ensemble as a solid-state nuclear spin gyroscope. Later in [29,30], quantum sensing of a rapid rotation (200 000 rpm) with a single NV electron spin was demonstrated. The potential for utilization of the nuclear spin was demonstrated recently [31,32]. However, the realization of a rotating sensor utilizing a nuclear spin ensemble in diamond remains a challenging task. In this Letter, we report the first proof-of-principle direct gyroscopic measurement of a sub-Hz rotation using double quantum Ramsey spectroscopy [33] of a hyperpolarized ^{14}N nuclear spin $I = 1$ ensemble in the solid state. Though the initial ideas were based on geometric Berry phase detection, here, we utilize dynamic phase acquisition as a result of a pseudomagnetic field induced by rotation [34].

All NV centers in diamond contain nitrogen nuclear spin, which in natural abundance is 99.6% ^{14}N with spin 1. Since nitrogen is part of the NV color center, it has a well-determined interaction with the NV electron spin [Fig. 1(a)]. Therefore, compared to the more developed nuclear spin of carbon-13, which is often believed to have better coherence and storage properties [35], the nuclear spin embedded into NV center nitrogen is suitable for ensemble measurements. Namely, using known techniques,
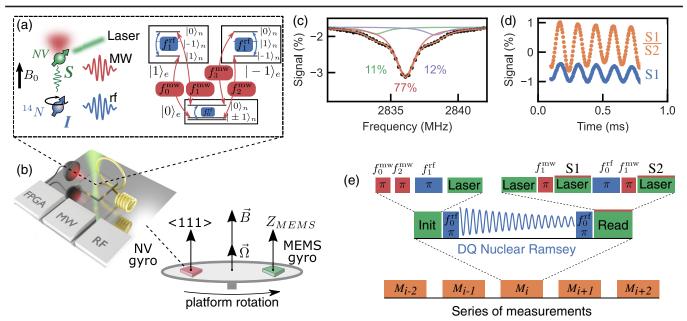
FIG. 1. Scheme of the experiment. (a) NV center in diamond associated with the nuclear spin of ^{14}N. It is addressed with laser light, MW, and rf control. The fluorescence of the NV center is collected using a photodiode. (b) The whole experimental setup with ensemble of NV centers inside a diamond plate is positioned on a rotation turntable to perform measurement of a calibrated rotation at various speeds. Crystallographic axis $\langle 111 \rangle$, bias magnetic field ($\vec{B}$), and MEMS sensitivity axis (Z_{MEMS}) are all aligned along rotation axis. NV centers of only $\langle 111 \rangle$ orientation are utilized in the measurement. (c) ODMR spectrum of the NV center ensemble with initialized nuclear spin. The nuclear spin is initialized before each frequency is measured. (d) Readout of the Ramsey nuclear spin. S1 and S2 are fluorescence signals normalized by laser intensity integrated during the first and second stage of nuclear readout [see panel (e)]. Signals are offset by 100%. Orange is the optimized referenced readout S1/S2, and blue is a simple S1 readout with only a single π pulse and a single laser pulse. (e) Measurement sequence for a gyroscopic measurement. Each measurement consists of an initialization step and nuclear spin free evolution in a scheme of double quantum interference. The free evolution is started by application a π pulse on the frequency f_0^{rf}.

one can polarize and readout nitrogen spin via the electron spin of an NV center spin [36]. The electron spin structure of the NV center ground state can be seen as a V-type scheme [see Fig. 1(a)] with the $m_S = 0$ subdomain as the lower state and $m_S = -1$ and $m_S = 1$ as the upper states. Nevertheless, each of these states has hyperfine splitting due to the interaction with the nitrogen nuclear spin, which can be described by the following Hamiltonian:

$$H = \hbar(S_z^2 + \gamma_e S_z B_z + S\mathbf{A}I + QI_z^2 + \gamma_n B_z I_z) \quad (1)$$

where D and Q are the zero-field splittings of the electron and nuclear spins, γ_e and γ_n are the gyromagnetic ratios of the electron and nuclear spin, S and I are spin operators for the spin 1 system, and $\mathbf{A}$ is the hyperfine tensor. Due to the different hyperfine splittings in electron spin subdomains, microwave (MW) transitions allow flipping of electron spin selectively on the nuclear spin state [36]. Similarly, radio frequency (rf) transitions can selectively flip nuclear spin. However, at small magnetic fields of ≈ 10 Gauss, the transition frequencies in $m_S = 0$ between $m_I = 0$ and $m_I = \pm 1$ are not resolved within the natural width of the transition and can be addressed with a single frequency pulse at $f_0^{rf} = |Q|/2\pi \approx 5$ MHz. Additionally, for $m_S = 1$

and $m_S = -1$, transitions from $m_I = 0$ to $m_I = 1$ and $m_I = -1$, respectively, have similar frequencies of approximately $f_1^{rf} = (|Q| + |A_{||}|)/2\pi \approx 7.2$ MHz and can be addressed with a single frequency pulse. We use this to perform effective control of the system using only two radio frequencies.

Our gyroscopic measurement consists of three main elements: nuclear spin polarization (lasts for 657 μs), free precession (1944 μs), and nuclear spin readout (193 μs). The polarization of the nuclear ensemble into the $m_I = 0$ spin state is performed using a recursive transfer of population [36–38] as depicted in Figs. 1(a) and 1(c). First, the populations of $|m_S = 0, m_I = \pm 1\rangle$ states are transferred to $|m_S = \pm 1, m_I = \pm 1\rangle$ states using spectrally narrow MW π pulses. Next, spectrally broad rf π pulse (28 μs) transfers both nuclear populations simultaneously to the $m_I = 0$ sublevel of the $|m_S = 1\rangle$ and $|m_S = -1\rangle$ states. Finally, a green laser pulse polarizes electronic spin so that the NV center is known to mostly populate the $|m_S = 0, m_I = 0\rangle$ state. This procedure is repeated four times to achieve the maximum population in the $m_I = 0$ state of $77 \pm 1\%$. Populations were defined from optically detected magnetic resonance (ODMR) spectrum [see Fig. 1(e)], fitted by three Lorentz contours. Amplitude of

each contour is directly proportional to the corresponding nuclear state population. Polarization efficiency is believed to be limited by decay of the nuclear polarization caused by an optical pumping pulse, required to prepare electron state $m_S = 0$. The underlying mechanism of this decay is believed to be electron-nuclear hyperfine interaction in excited state [37–39].

The rotation of the setup around the main quantization axis of the NV center ensemble ($\langle 111 \rangle$ axis of the diamond) is analogous to the introduction of a pseudomagnetic field [34], where the nuclear spin behavior is described by the Hamiltonian:

$$H_0 = \hbar(QI_z^2 + \gamma_n B_z I_z + \Omega I_z). \tag{2}$$

To acquire a rotation signal, we monitor the free precession of the ^{14}N nuclear spin ensemble in the electron spin $m_S = 0$ subdomain of the NV center ground state [Fig. 1(e)]. Free precession of the nuclear spin after initialization is started with a broadband radio frequency π pulse (19 μs) of frequency $f_0^{\mathrm{rf}} = |Q|/2\pi$ [Fig. 2(a)], which brings the nuclear spin into the "bright" superposition state $|b\rangle = (|1\rangle + |-1\rangle)/\sqrt{2}$. During the free evolution under the Hamiltonian H_0, this state acquires a phase $\phi = 2(\gamma_n B_z + \Omega)\tau$ due to the energy splitting between the $m_I = \pm 1$ sublevels. The state after the free evolution can be expressed as $(e^{i\phi}|1\rangle + e^{-i\phi}|-1\rangle)/\sqrt{2} = (\cos\phi|b\rangle + i\sin\phi|d\rangle)/\sqrt{2}$, where $|d\rangle = (|1\rangle - |-1\rangle)/\sqrt{2}$
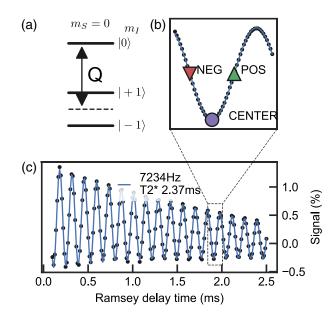

FIG. 2. Rotation signal. (a) DQ Ramsey transition scheme for $m_S = 0$. (b) Enlarged Ramsey fringe at working point of the gyroscope. Working points for alternating Ramsey protocol are marked as NEG on the native slope and POS on the positive slope. (c) DQ Ramsey spectroscopy of ^{14}N nuclear spin. The oscillation matches the nuclear Zeeman splitting, $T_2^* = 2.37$ ms.

denotes the "dark" state. The last π pulse converts the bright state back to $|0\rangle$, while the dark state remains unchanged.

To perform readout of thus prepared state laser pulse repolarizes electron spin into state $|m_S = 0\rangle$ and at the same time destroys phase of the $|d\rangle$ state. To measure $|m_I = 0\rangle$ component its population is moved into $|m_S = 1\rangle$ state using selective π pulse at frequency f_1^{MW}. Then laser pulse is applied to read fluorescence (signal S1) and to repolarize electron spin back to $|m_S = 0\rangle$. To measure sum of $|m_I = \pm 1\rangle$ states it is swapped with $|m_I = 0\rangle$ using π pulse of frequency f_0^{rf} and then readout of $|m_I = 0\rangle$ is repeated (signal S2). The S1 and S2 signals are linear functions of the $|b\rangle$ and $|d\rangle$ state and their ratio reveals full population difference between $|b\rangle$ and $|d\rangle$ states [see Fig. 1(d)].

The experimental double quantum Ramsey precession of ^{14}N is shown in Figs. 2(b) and 2(c). It is fitted with a decaying sinusoidal curve with $T_2^* = 2.37$ ms. By fixing a working point at $\tau = 2$ ms, we recalculate the rotation signal from the measured fluorescence [Fig. 2(b)] and magnetic field:

$$\Omega = \frac{1}{a(t_p + t_n)}(S_p - S_n) - \gamma_n \Delta B_z. \tag{3}$$

Here ΔB_z is the change in externally applied magnetic field, $a = 0.5(S_{\max} - S_{\min})$ is the amplitude of Ramsey fringes at the selected interrogation time, S_p and S_n denotes the signals taken at negative and positive slope of the Ramsey fringe around the working points t_p and t_n. Both slopes are used to remove the uncertainties due to the low frequency noise related to the initialization fidelity of the nuclear spin and the fidelity of the π pulses (see the Supplemental Material [40], Sec. IV and Table II).

Due to the laser irradiation and electrical current in nearby antennas, the diamond sample unavoidably heats up. Temperature shifts affect both electron [41] and nuclear hyperfine terms in the Hamiltonian as in [42–44]. In addition, the position of the ODMR resonances is also sensitive to stray external magnetic fields, which may change over time. Thus, the sensor requires compensation of these temperature- and magnetic field-induced shifts. To realize this, the temperature and magnetic field were measured in interleaved mode using the same NV ensemble similar to [32]. In our case, we implemented continuous wave (CW) ODMR measurement with digital frequency modulation to measure both magnetic transitions [40]. Sweeping microwave offset frequency provided ODMR derivative curve [Fig. 3(a)]. Linear central part of the curve gives calibration data to deduce actual frequencies f_1^{MW}, f_3^{MW} corresponding to transitions $|m_S = 0, m_I = 0\rangle \leftrightarrow |m_S = \pm 1, m_I = 0\rangle$. Magnetic field amplitude B_z can be calculated from Zeeman splitting between $|m_S = \pm 1\rangle$ using the formula $B_z = (f_1^{\mathrm{MW}} - f_3^{\mathrm{MW}})/2\gamma_e$. To estimate comagnetometer sensitivity we run continuous magnetic field measure-
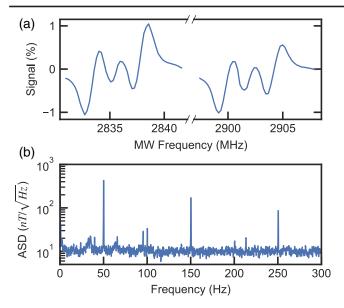
FIG. 3. Comagnetometer and cothermometer performance. (a) ESR dispersion contour when scanning the $m_S = -1$ and $m_S = 1$ electron spin transitions. (b) Amplitude spectral density (ASD) of a free running comagnetometer at zero rotation rate.

ment and plot Fourier spectrum of obtained B_z signal [see Fig. 3(b)]. The sensitivity of such a realized comagnetometer has a noise floor of 10 nT/$\sqrt{\text{Hz}}$, which corresponds to a rotation measurement noise floor of 11 deg/s/$\sqrt{\text{Hz}}$ [40]. The magnetic field and temperature measurements were performed between two sequential gyroscopic measurements, and their results were used as feedback to subtract the corresponding systematic noise in the rotation sensor [40]. Having at hand information about both ESR transitions, we also realized a cothermometer and compensated for the temperature-related shifts [40].

Demonstration of a proof-of-principle gyroscope sensor is a challenging task since the whole experimental setup should be rotated. Vibrational mechanical noise could reduce the optical signal-to-noise ratio, thus causing degradation of the performance of the sensor. To avoid difficulties with rotational electrical and optical joints, we employed full rotation of the optical setup and all devices in use. To this end, we assembled an experimental setup that can autonomously operate on a rotation stage [see Fig. 1(b)]. It is equipped with a battery power supply, wireless communication protocols, field programmable gate arrays a control board, a laptop, and all MW, rf, and optical equipment required for operation [40].

To calibrate our sensor, a series of continuous rotations with various rotation speeds in both directions were performed [see Figs. 4(a) and 4(b)]. We obtained a series of measurements from the comagnetometer, cothermometer, gyroscope, and calibration MEMS gyroscope, which
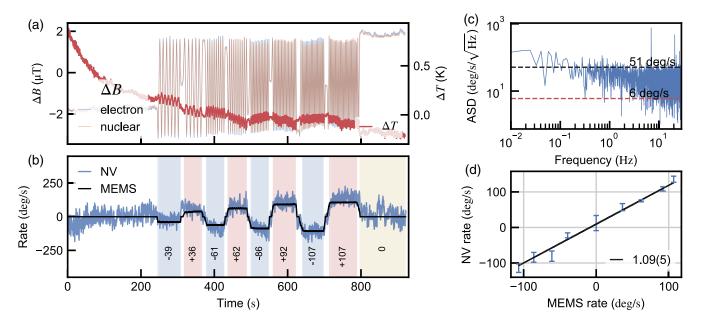

FIG. 4. Calibration measurement on a rotation stage. (a) Sensing of rotation parameters on the rotation table. Data of a comagnetometer and a cothermometer in various rotation regimes. "Electron" curve corresponds to CW-ODMR comagnetometer data. "Nuclear" curve is magnetic field change, deduced from nuclear Ramsey beating frequency change. (b) Sample MEMS gyro and rotation signal from the NV gyro. The black solid curve is the sampling value of a commercial MEMS gyroscope, and the blue solid line is the NV gyro sensor output. Shaded areas represent the averaging times for rotation measurements (see [40] for details) with numbers in the bottom corresponding to averaged MEMS rate (deg /s). (c) ASD of noise of the sensor output estimated in the last part of the measurement run, where the rotation speed was zero. The red curve is the estimation of the ASD based on the photon shot noise of the detected fluorescence. The black dashed curve is the noise floor of the NV-based sensor. (d) NV gyroscope signal output at various rotation rates of the moving stage. The error bars were taken from Allan deviation minimum for NV gyroscope signal within averaging segment. We note a linear character of the rotation signal dependence as a MEMS rotation signal output with a slope of 1.09(5).

are depicted in Figs. 4(a) and 4(b). As clearly seen, the results of the calibration MEMS gyroscope clearly correlate with the outputs of our NV-based gyroscope sensor. The obtained rotation signal is linearly proportional to the real rotation speed, as depicted in Fig. 4(d). The scaling factor estimated from the experiment is 1.09(5). The noise floor of our NV gyroscope was measured to be 52 $\deg/s/\sqrt{Hz}$ [see Fig. 4(c)], which was estimated as the noise floor of the power spectral density of the time trace of the gyro output.

To further improve the sensitivity of the gyro prototype several improvements to setup could be implemented. On the technical side current realization fluorescence detection scheme was not optimized and could be improved to reach shot noise performance [45]. Second, the efficiency of photoconversion could be improved with the help of total internal reflection light guiding [46]. Additionally, polarization and readout of nuclear spins could be improved via optimization of laser wavelength[47], or excited state level anticrossing technique [43,48]. Also, the material properties should be optimized towards better T_2 times of the nuclear ensemble limited with electron spin T_1^e. These factors could lead to the total improvement in sensitivity by factor of 800 (see [40] for details). To improve the long-term performance of the sensor, an important step would be to include both passive and active temperature and magnetic field stabilization. The latter should have sensitivity of at least 60 $pT/\sqrt{Hz}$ to achieve the 800-fold improvement mentioned above. Finally, schemes that implement coherent magnetic field feedback [49] or utilize double species nuclear ensembles such as in [15] would result in ultimate robustness of the device against magnetic field fluctuations.

We showed a direct signal of rotation measured with a realized nuclear spin gyroscope based on an ensemble of NV centers in diamond. By simultaneously measuring the magnetic field and temperature, we subtracted the systematic shifts from the rotation signal and obtained a linear calibration curve of the rotation signal. This results together with a previous demonstration of long-term stability on a nonrotating device [32] proves the possibility of measuring rotation using nuclear spins of an ensemble of NV centers in diamond and paves the way for low drift compact solid-state gyroscopes.

---

*akimov@physics.tamu.edu

[1] G. Mattei, F. Scibona, L. Rosa, M. Lucchesini, A. Esposito, and D. Tonelli, An advanced itar-free INS/GPS designed and developed in Italy, in *XXV International Congress Of Aeronautics And Astronautics, Italian Association of Aeronautics and Astronautics* (2019), https://www.aidaa2019.com/.

[2] F. Vanegas and F. Gonzalez, Enabling UAV navigation with sensor and environmental uncertainty in cluttered and GPS-denied environments, Sensors **16**, 666 (2016).

[3] A. Khattab, Y. A. Fahmy, and A. A. Wahab, High accuracy GPS-free vehicle localization framework via an ins-assisted single RSU, Int. J. Distributed Sensor Netw. **11**, 795036 (2015).

[4] C. Etrich, P. Mandel, R. Centeno Neelen, R. J. C. Spreeuw, and J. P. Woerdman, Dynamics of a ring-laser gyroscope with backscattering, Phys. Rev. A **46**, 525 (1992).

[5] C. M. Ferrar, Progress in fiber optic gyro development, in *34th International Instrumentation Symposium, Instrument Society of America* (1988), pp. 189–198, https://ui.adsabs.harvard.edu/abs/1988isa..symp..189F/abstract.

[6] R. A. Bergh, H. C. Lefèvre, and H. J. Shaw, All single mode fiber optic gyroscope, Opt. Lett. **6**, 198 (1981).

[7] H. C. Lefèvre, The fiber-optic gyroscope, a century after Sagnac's experiment: The ultimate rotation-sensing technology?, C.R. Phys. **15**, 851 (2014).

[8] H. Lefèvre, *The Fiber-Optic Gyroscope, Second Edition* (Artech House, Boston, 2014), ISBN-13: 978-1-60807-695-6.

[9] H. J. Arditty and H. C. Lefèvre, Sagnac effect in fiber gyroscopes, Opt. Lett. **6**, 401 (1981).

[10] M. G. Sagnac and M. E. Bouty, L'éther lumineux démontré par l'effet du vent relatif d'éther dans un interféromètre en rotation uniforme, De L'académie des Sciences **95**, 708 (1913), https://gallica.bnf.fr/ark:/12148/bpt6k31103/f709.item.

[11] Y. H. Lai, M. G. Suh, Y. K. Lu, B. Shen, Q. F. Yang, H. Wang, J. Li, S. H. Lee, K. Y. Yang, and K. Vahala, Earth rotation measured by a chip-scale ring laser gyroscope, Nat. Photonics **14**, 345 (2020).

[12] V. M. N. Passaro, A. Cuccovillo, L. Vaiani, M. D. Carlo, and C. E. Campanella, Gyroscope technology and applications: A review in the industrial perspective, Sensors **17**, 2284 (2017).

[13] K. Y. Yang, D. Y. Oh, S. H. Lee, Q. F. Yang, X. Yi, B. Shen, H. Wang, and K. Vahala, Bridging ultrahigh-Q devices and photonic circuits, Nat. Photonics **12**, 297 (2018).

[14] K. F. Woodman, P. W. Franks, and M. D. Richards, The nuclear magnetic resonance gyroscope—A review, J. Navig. **40**, 366 (1987).

[15] T. W. Kornack, R. K. Ghosh, and M. V. Romalis, Nuclear Spin Gyroscope Based on an Atomic Comagnetometer, Phys. Rev. Lett. **95**, 230801 (2005).

[16] T. G. Walker and M. S. Larsen, Spin-exchange-pumped NMR gyros, Adv. At. Mol. Opt. Phys. **65**, 373 (2016).

[17] A. K. Vershovskii, Y. A. Litmanovich, A. S. Pazgalev, and V. G. Peshekhonov, Nuclear magnetic resonance gyro: Ultimate parameters, Gyrosc. Navig. **9**, 162 (2018).

[18] K. Zhang, N. Zhao, and Y.-H. Wang, Closed-loop nuclear magnetic resonance gyroscope based on Rb-Xe, Sci. Rep. **10**, 2258 (2020).

[19] N. Aslam, M. Pfender, P. Neumann, R. Reuter, A. Zappe, F. F. De Oliveira, A. Denisenko, H. Sumiya, S. Onoda, J. Isoya, and J. Wrachtrup, Nanoscale nuclear magnetic resonance with chemical resolution, Science **357**, 67 (2017).

[20] D. R. Glenn, D. B. Bucher, J. Lee, M. D. Lukin, H. Park, and R. L. Walsworth, High-resolution magnetic resonance spectroscopy using a solid-state spin sensor, Nature (London) **555**, 351 (2018).

[21] T. Wolf, P. Neumann, K. Nakamura, H. Sumiya, T. Ohshima, J. Isoya, and J. Wrachtrup, Subpicotesla Diamond Magnetometry, Phys. Rev. X **5**, 041001 (2015).

[22] J. M. Schloss, J. F. Barry, M. J. Turner, and R. L. Walsworth, Simultaneous Broadband Vector Magnetometry Using Solid-State Spins, Phys. Rev. Applied **10**, 034044 (2018).

[23] P. Maletinsky, S. Hong, M. S. Grinolds, B. Hausmann, M. D. Lukin, R. L. Walsworth, M. Loncar, and A. Yacoby, A robust scanning diamond sensor for nanoscale imaging with single nitrogen-vacancy centres, Nat. Nanotechnol. **7**, 320 (2012).

[24] F. Dolde, H. Fedder, M. W. Doherty, T. Nöbauer, F. Rempp, G. Balasubramanian, T. Wolf, F. Reinhard, L. C. Hollenberg, F. Jelezko, and J. Wrachtrup, Electric-field sensing using single diamond spins, Nat. Phys. **7**, 459 (2011).

[25] G. Kucsko, P. C. Maurer, N. Y. Yao, M. Kubo, H. J. Noh, P. K. Lo, H. Park, and M. D. Lukin, Nanometre-scale thermometry in a living cell, Nature (London) **500**, 54 (2013).

[26] M. P. Ledbetter, K. Jensen, R. Fischer, A. Jarmola, and D. Budker, Gyroscopes based on nitrogen-vacancy centers in diamond, Phys. Rev. A **86**, 052116 (2012).

[27] A. Ajoy and P. Cappellaro, Stable three-axis nuclear-spin gyroscope in diamond, Phys. Rev. A **86**, 062104 (2012).

[28] D. Maclaurin, M. W. Doherty, L. C. L. Hollenberg, and A. M. Martin, Measurable Quantum Geometric Phase from a Rotating Single Spin, Phys. Rev. Lett. **108**, 240403 (2012).

[29] A. A. Wood, E. Lilette, Y. Y. Fein, N. Tomek, L. P. McGuinness, L. C. L. Hollenberg, R. E. Scholten, and A. M. Martin, Quantum measurement of a rapidly rotating spin qubit in diamond, Sci. Adv. **4**, eaar7691 (2018).

[30] A. A. Wood, L. C. Hollenberg, R. E. Scholten, and A. M. Martin, Observation of a Quantum Phase from Classical Rotation of a Single Spin, Phys. Rev. Lett. **124**, 20401 (2020).

[31] A. A. Wood, E. Lilette, Y. Y. Fein, V. S. Perunicic, L. C. Hollenberg, R. E. Scholten, and A. M. Martin, Magnetic pseudo-fields in a rotating electron-nuclear spin system, Nat. Phys. **13**, 1070 (2017).

[32] J. C. Jaskula, K. Saha, A. Ajoy, D. J. Twitchen, M. Markham, and P. Cappellaro, Cross-Sensor Feedback Stabilization of an Emulated Quantum Spin Gyroscope, Phys. Rev. Applied **11**, 1 (2019).

[33] H. J. Mamin, M. H. Sherwood, M. Kim, C. T. Rettner, K. Ohno, D. D. Awschalom, and D. Rugar, Multipulse Double-Quantum Magnetometry with Near-Surface Nitrogen-Vacancy Centers, Phys. Rev. Lett. **113**, 030803 (2014).

[34] R. Tycko, Adiabatic Rotational Splittings and Berry's Phase in Nuclear Quadrupole Resonance, Phys. Rev. Lett. **58**, 2281 (1987).

[35] P. C. Maurer, G. Kucsko, C. Latta, L. Jiang, N. Y. Yao, S. D. Bennett, F. Pastawski, D. Hunger, N. Chisholm, M. Markham, D. J. Twitchen, J. I. Cirac, and M. D. Lukin,

Room-temperature quantum bit memory exceeding one Second, Science **336**, 1283 (2012).

[36] B. Smeltzer, J. McIntyre, and L. Childress, Robust control of individual nuclear spins in diamond, Phys. Rev. A **80**, 050302 (2009).

[37] D. Pagliero, A. Laraoui, J. D. Henshaw, and C. A. Meriles, Recursive polarization of nuclear spins in diamond at arbitrary magnetic fields, Appl. Phys. Lett. **105**, 242402 (2014).

[38] T. Chakraborty, J. Zhang, and D. Suter, Polarizing the electronic and nuclear spin of the NV-center in diamond in arbitrary magnetic fields: Analysis of the optical pumping process, New J. Phys. **19**, 073030 (2017).

[39] P. Neumann, J. Beck, M. Steiner, F. Rempp, H. Fedder, P. R. Hemmer, J. Wrachtrup, and F. Jelezko, Single-shot readout of a single nuclear spin, Science **329**, 542 (2010).

[40] See the Supplemental Material at http://link.aps.org/supplemental/10.1103/PhysRevLett.126.197702 for details on Comagnetometer, Cothermometer; Nuclear spin readout; Temperature compensation; Equivalent magnetic field for the rotation rate; Recalculation of the rotation signal from fluorescence; Rotation measurements; Setup details; Shot noise estimation; Sensitivity improvement.

[41] V. M. Acosta, E. Bauch, M. P. Ledbetter, A. Waxman, L. S. Bouchard, and D. Budker, Temperature Dependence of the Nitrogen-Vacancy Magnetic Resonance in Diamond, Phys. Rev. Lett. **104**, 070801 (2010).

[42] V. V. Soshenko, V. V. Vorobyov, S. V. Bolshedvorskii, O. Rubinas, I. Cojocaru, B. Kudlatsky, A. I. Zeleneev, V. N. Sorokin, A. N. Smolyaninov, and A. V. Akimov, Temperature drift rate for nuclear terms of the nv-center ground-state hamiltonian, Phys. Rev. B **102**, 125133 (2020).

[43] A. Jarmola, I. Fescenko, V. M. Acosta, M. W. Doherty, F. K. Fatemi, T. Ivanov, D. Budker, and V. S. Malinovsky, Robust optical readout and characterization of nuclear spin transitions in nitrogen-vacancy ensembles in diamond, Phys. Rev. Research **2**, 023094 (2020).

[44] M. S. Barson, P. Reddy, S. Yang, N. B. Manson, J. Wrachtrup, and M. W. Doherty, Temperature dependence of the C 13 hyperfine structure of the negatively charged nitrogen-vacancy center in diamond, Phys. Rev. B **99**, 094101 (2019).

[45] P. C. D. Hobbs, Ultrasensitive laser measurements without tears, Appl. Opt. **36**, 903 (1997).

[46] H. Clevenson, M. E. Trusheim, T. Schroder, C. Teale, D. Braje, and D. Englund, Broadband magnetometry and temperature sensing with a light trapping diamond waveguide, Nat. Phys. **11**, 393 (2015).

[47] K. R. K. Rao, Y. Wang, J. Zhang, and D. Suter, Optimal photon energies for initialization of hybrid spin quantum registers of nitrogen-vacancy centers in diamond, Phys. Rev. A **101**, 013835 (2020).

[48] R. Fischer, A. Jarmola, P. Kehayias, and D. Budker, Optical polarization of nuclear ensembles in diamond, Phys. Rev. B **87**, 125207 (2013).

[49] M. Hirose and P. Cappellaro, Coherent feedback control of a single qubit in diamond, Nature (London) **532**, 77 (2016).